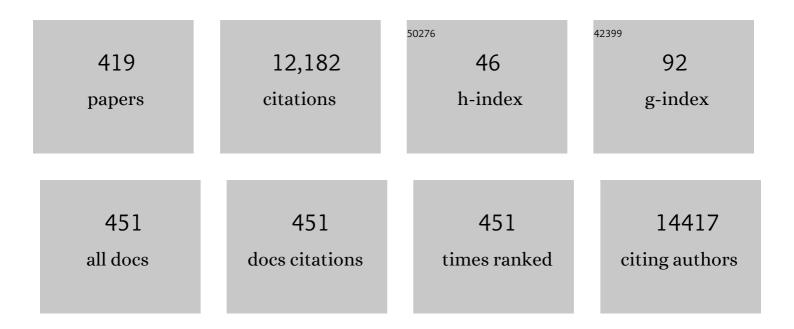
List of Publications by Year in descending order

Source: https://exaly.com/author-pdf/350908/publications.pdf Version: 2024-02-01



3

#	Article	IF	CITATIONS
1	Altered gray matter development in preâ€reading children with a family history of reading disorder. Developmental Science, 2022, 25, e13160.	2.4	8
2	Axonal Injury Partially Mediates Associations Between Increased Left Ventricular Mass Index and White Matter Damage. Stroke, 2022, 53, 808-816.	2.0	0
3	TractEM: Evaluation of protocols for deterministic tractography white matter atlas. Magnetic Resonance Imaging, 2022, 85, 44-56.	1.8	1
4	Lower cerebral oxygen utilization is associated with Alzheimer's disease-related neurodegeneration and poorer cognitive performance among apolipoprotein E ε4 carriers. Journal of Cerebral Blood Flow and Metabolism, 2022, 42, 642-655.	4.3	3
5	Structural MRI-Based Measures of Accelerated Brain Aging do not Moderate the Acute Antidepressant Response in Late-Life Depression. American Journal of Geriatric Psychiatry, 2022, 30, 1015-1025.	1.2	7
6	Circle Representation for Medical Object Detection. IEEE Transactions on Medical Imaging, 2022, 41, 746-754.	8.9	20
7	Generalizing deep learning brain segmentation for skull removal and intracranial measurements. Magnetic Resonance Imaging, 2022, 88, 44-52.	1.8	4
8	pyPheWAS: A Phenome-Disease Association Tool for Electronic Medical Record Analysis. Neuroinformatics, 2022, 20, 483-505.	2.8	9
9	Learning white matter subjectâ \in specific segmentation from structural MRI. Medical Physics, 2022, , .	3.0	4
10	Tractostorm 2: Optimizing tractography dissection reproducibility with segmentation protocol dissemination. Human Brain Mapping, 2022, 43, 2134-2147.	3.6	8
11	Workflow Integration of Research AI Tools into a Hospital Radiology Rapid Prototyping Environment. Journal of Digital Imaging, 2022, , 1.	2.9	0
12	Accelerated decline in white matter microstructure in subsequently impaired older adults and its relationship with cognitive decline. Brain Communications, 2022, 4, fcac051.	3.3	16
13	Multimodal neuroimaging in pediatric type 1 diabetes: a pilot multisite feasibility study of acquisition quality, motion, and variability. , 2022, , .		1
14	Extending the value of routine lung screening CT with quantitative body composition assessment. , 2022, , .		2
15	Longitudinal changes of connectomes and graph theory measures in aging. , 2022, 12032, .		2
16	Supervised deep generation of high-resolution arterial phase computed tomography kidney substructure atlas. , 2022, , .		0
17	Joint independent component analysis for hypothesizing spatiotemporal relationships between longitudinal gray and white matter changes in preclinical Alzheimer's disease. , 2022, , .		0

18 Ultra-high-resolution mapping of cortical layers 3T-guided 7T MRI. , 2022, , .

2

#	Article	IF	CITATIONS
19	Efficient quality control with mixed CT and CTA datasets. , 2022, , .		0
20	Inpainting missing tissue in multiplexed immunofluorescence imaging. , 2022, 12039, .		0
21	Mapping the impact of non-linear gradient fields on diffusion MRI tensor estimation. , 2022, , .		0
22	An atlas of white matter anatomy, its variability, and reproducibility based on constrained spherical deconvolution of diffusion MRI. NeuroImage, 2022, 254, 119029.	4.2	23
23	Prevalence of white matter pathways coming into a single white matter voxel orientation: The bottleneck issue in tractography. Human Brain Mapping, 2022, 43, 1196-1213.	3.6	34
24	Longitudinal associations of absolute versus relative moderate-to-vigorous physical activity with brain microstructural decline in aging. Neurobiology of Aging, 2022, 116, 25-31.	3.1	5
25	Enabling Al innovation via data and model sharing: An overview of the NSF Convergence Accelerator Track D. Al Magazine, 2022, 43, 93-104.	1.6	2
26	The impact of the lung EDRN-CVC on Phase 1, 2, & 3 biomarker validation studies. Cancer Biomarkers, 2022, 33, 449-465.	1.7	0
27	Multi-contrast computed tomography healthy kidney atlas. Computers in Biology and Medicine, 2022, 146, 105555.	7.0	4
28	Label efficient segmentation of single slice thigh CT with two-stage pseudo labels. Journal of Medical Imaging, 2022, 9, .	1.5	5
29	EPI susceptibility correction introduces significant differences far from local areas of high distortion. Magnetic Resonance Imaging, 2022, 92, 1-9.	1.8	4
30	Aging and white matter microstructure and macrostructure: a longitudinal multi-site diffusion MRI study of 1218 participants. Brain Structure and Function, 2022, 227, 2111-2125.	2.3	25
31	Insights from the IronTract challenge: Optimal methods for mapping brain pathways from multi-shell diffusion MRI. NeuroImage, 2022, 257, 119327.	4.2	17
32	The influence of regions of interest on tractography virtual dissection protocols: general principles to learn and to follow. Brain Structure and Function, 2022, 227, 2191-2207.	2.3	5
33	Contrastive semi-supervised harmonization of single-shell to multi-shell diffusion MRI. Magnetic Resonance Imaging, 2022, 93, 73-86.	1.8	5
34	The Medical Segmentation Decathlon. Nature Communications, 2022, 13, .	12.8	252
35	Lower cardiac output is associated with neurodegeneration among older adults with normal cognition but not mild cognitive impairment. Brain Imaging and Behavior, 2021, 15, 2040-2050.	2.1	3
36	Pandora: 4-D White Matter Bundle Population-Based Atlases Derived from Diffusion MRI Fiber Tractography. Neuroinformatics, 2021, 19, 447-460.	2.8	15

#	Article	lF	CITATIONS
37	Hippocampal activation and connectivity in the aging brain. Brain Imaging and Behavior, 2021, 15, 711-726.	2.1	15
38	Using phecode analysis to characterize co-occurring medical conditions in autism spectrum disorder. Autism, 2021, 25, 800-811.	4.1	12
39	Empirical field mapping for gradient nonlinearity correction of multi-site diffusion weighted MRI. Magnetic Resonance Imaging, 2021, 76, 69-78.	1.8	10
40	High-resolution 3D abdominal segmentation with random patch network fusion. Medical Image Analysis, 2021, 69, 101894.	11.6	26
41	Phase identification for dynamic CT enhancements with generative adversarial network. Medical Physics, 2021, 48, 1276-1285.	3.0	4
42	The relationship between white matter microstructure and self-perceived cognitive decline. NeuroImage: Clinical, 2021, 32, 102794.	2.7	9
43	MRI network progression in mesial temporal lobe epilepsy related to healthy brain architecture. Network Neuroscience, 2021, 5, 434-450.	2.6	9
44	Joint cortical surface and structural connectivity analysis of Alzheimer's disease. , 2021, 11596, .		2
45	Joint analysis of structural connectivity and cortical surface features: correlates with mild traumatic brain injury. , 2021, 11596, .		0
46	A cross-platform informatics system for the Gut Cell Atlas: integrating clinical, anatomical and histological data. , 2021, 11601, .		4
47	Validation and estimation of spleen volume via computer-assisted segmentation on clinically acquired CT scans. Journal of Medical Imaging, 2021, 8, 014004.	1.5	4
48	Prenatal and postnatal maternal anxiety and amygdala structure and function in young children. Scientific Reports, 2021, 11, 4019.	3.3	33
49	Deep multi-path network integrating incomplete biomarker and chest CT data for evaluating lung cancer risk. , 2021, 11596, .		6
50	Construction of a multi-phase contrast computed tomography kidney atlas. , 2021, 11596, .		1
51	On statistical tests of functional connectome fingerprinting. Canadian Journal of Statistics, 2021, 49, 63-88.	0.9	8
52	Establishing surface correspondence for post-surgical cortical thickness changes in temporal lobe epilepsy. , 2021, 11596, .		1
53	Development and characterization of a chest CT atlas. , 2021, 2021, .		1
54	Renal cortex, medulla and pelvicaliceal system segmentation on arterial phase CT images with random patch-based networks. , 2021, 11596, .		3

#	Article	IF	CITATIONS
55	PreQual: An automated pipeline for integrated preprocessing and quality assurance of diffusion weighted MRI images. Magnetic Resonance in Medicine, 2021, 86, 456-470.	3.0	43
56	Validation of group-wise registration for surface-based functional MRI analysis. , 2021, 11596, .		1
57	Measure partial liver volumetric variations from paired inspiratory-expiratory chest CT scans. , 2021, 11596, .		0
58	Anatomical texture patterns identify cerebellar distinctions between essential tremor and Parkinson's disease. Human Brain Mapping, 2021, 42, 2322-2331.	3.6	10
59	Dispositional Negative Emotionality in Childhood and Adolescence Predicts Structural Variation in the Amygdala and Caudal Anterior Cingulate During Early Adulthood: Theoretically and Empirically Based Tests. Research on Child and Adolescent Psychopathology, 2021, 49, 1275-1288.	2.3	3
60	Rap-Net: Coarse-To-Fine Multi-Organ Segmentation With Single Random Anatomical Prior. , 2021, 2021, 1491-1494.		3
61	Labeling lateral prefrontal sulci using spherical data augmentation and context-aware training. Neurolmage, 2021, 229, 117758.	4.2	19
62	Multi-Site Infant Brain Segmentation Algorithms: The iSeg-2019 Challenge. IEEE Transactions on Medical Imaging, 2021, 40, 1363-1376.	8.9	53
63	Body Part Regression With Self-Supervision. IEEE Transactions on Medical Imaging, 2021, 40, 1499-1507.	8.9	10
64	Cortical Morphology in Autism: Findings from a Cortical Shape-Adaptive Approach to Local Gyrification Indexing. Cerebral Cortex, 2021, 31, 5188-5205.	2.9	6
65	MASiVar: Multisite, multiscanner, and multisubject acquisitions for studying variability in diffusion weighted MRI. Magnetic Resonance in Medicine, 2021, 86, 3304-3320.	3.0	16
66	Faster Mean-shift: GPU-accelerated clustering for cosine embedding-based cell segmentation and tracking. Medical Image Analysis, 2021, 71, 102048.	11.6	150
67	Default mode network connectivity and cognition in the aging brain: the effects of age, sex, and APOE genotype Neurobiology of Aging, 2021, 104, 10-23.	3.1	12
68	Integrated Biomarkers for the Management of Indeterminate Pulmonary Nodules. American Journal of Respiratory and Critical Care Medicine, 2021, 204, 1306-1316.	5.6	36
69	Comparison of convolutional neural networks for detecting large vessel occlusion on computed tomography angiography. Medical Physics, 2021, 48, 6060-6068.	3.0	7
70	Mapping gradient nonlinearity and miscalibration using diffusionâ€weighted MR images of a uniform isotropic phantom. Magnetic Resonance in Medicine, 2021, 86, 3259-3273.	3.0	8
71	Automated, open-source segmentation of the Hippocampus and amygdala with the open Vanderbilt archive of the temporal lobe. Magnetic Resonance Imaging, 2021, 81, 17-23.	1.8	3
72	Diminishing Uncertainty Within the Training Pool: Active Learning for Medical Image Segmentation. IEEE Transactions on Medical Imaging, 2021, 40, 2534-2547.	8.9	28

#	Article	IF	CITATIONS
73	Fiber tractography bundle segmentation depends on scanner effects, vendor effects, acquisition resolution, diffusion sampling scheme, diffusion sensitization, and bundle segmentation workflow. NeuroImage, 2021, 242, 118451.	4.2	35
74	Tractography dissection variability: What happens when 42 groups dissect 14 white matter bundles on the same dataset?. NeuroImage, 2021, 243, 118502.	4.2	94
75	Lung Cancer Risk Estimation with Incomplete Data: A Joint Missing Imputation Perspective. Lecture Notes in Computer Science, 2021, , 647-656.	1.3	4
76	Methods and open-source toolkit for analyzing and visualizing challenge results. Scientific Reports, 2021, 11, 2369.	3.3	25
77	Cancer Risk Estimation Combining Lung Screening CT with Clinical Data Elements. Radiology: Artificial Intelligence, 2021, 3, e210032.	5.8	8
78	Deterministic inverse design of Tamm plasmon thermal emitters with multi-resonant control. Nature Materials, 2021, 20, 1663-1669.	27.5	46
79	Elevated Aortic Pulse Wave Velocity Relates to Longitudinal Gray and White Matter Changes. Arteriosclerosis, Thrombosis, and Vascular Biology, 2021, 41, 3015-3024.	2.4	9
80	Brief Report: The Characterization of Medical Comorbidity Prior to Autism Diagnosis in Children Before Age Two. Journal of Autism and Developmental Disorders, 2021, , 1.	2.7	1
81	Apolipoprotein ε genotype modifies the association between bloodâ€brain barrier permeability and both grey and white matter integrity in older adults. Alzheimer's and Dementia, 2021, 17, .	0.8	0
82	Random Multi-Channel Image Synthesis for Multiplexed Immunofluorescence Imaging Proceedings of Machine Learning Research, 2021, 156, 36-46.	0.3	0
83	Medial temporal lobe volumes in late-life depression: effects of age and vascular risk factors. Brain Imaging and Behavior, 2020, 14, 19-29.	2.1	14
84	Brainstem Functional Connectivity Disturbances in Epilepsy may Recover After Successful Surgery. Neurosurgery, 2020, 86, 417-428.	1.1	12
85	Tractography reproducibility challenge with empirical data (TraCED): The 2017 ISMRM diffusion study group challenge. Journal of Magnetic Resonance Imaging, 2020, 51, 234-249.	3.4	38
86	Distributed deep learning across multisite datasets for generalized CT hemorrhage segmentation. Medical Physics, 2020, 47, 89-98.	3.0	28
87	Anatomical context protects deep learning from adversarial perturbations in medical imaging. Neurocomputing, 2020, 379, 370-378.	5.9	29
88	Multiatlas segmentation. , 2020, , 137-164.		2
89	Accelerated brain aging predicts impaired cognitive performance and greater disability in geriatric but not midlife adult depression. Translational Psychiatry, 2020, 10, 317.	4.8	37
90	BIAS: Transparent reporting of biomedical image analysis challenges. Medical Image Analysis, 2020, 66, 101796.	11.6	59

#	Article	IF	CITATIONS
91	Cross-scanner and cross-protocol multi-shell diffusion MRI data harmonization: Algorithms and results. NeuroImage, 2020, 221, 117128.	4.2	54
92	Microstructural Neuroimaging of Frailty in Cognitively Normal Older Adults. Frontiers in Medicine, 2020, 7, 546344.	2.6	14
93	Distortion correction of diffusion weighted MRIÂwithout reverse phase-encoding scans or field-maps. PLoS ONE, 2020, 15, e0236418.	2.5	60
94	Lasting consequences of concussion on the aging brain: Findings from the Baltimore Longitudinal Study of Aging. Neurolmage, 2020, 221, 117182.	4.2	11
95	BRAIN AGE ESTIMATION IN LATE-LIFE DEPRESSION: ASSOCIATION WITH COGNITIVE PERFORMANCE AND DISABILITY. American Journal of Geriatric Psychiatry, 2020, 28, S88-S89.	1.2	0
96	Time-distanced gates in long short-term memory networks. Medical Image Analysis, 2020, 65, 101785.	11.6	21
97	Capturing Intra-Scanner and Inter-Scanner Variability in Quantitative MR: Effect on Neuroimaging Studies. Biological Psychiatry, 2020, 87, S55-S56.	1.3	0
98	Association of Poorer Hearing With Longitudinal Change in Cerebral White Matter Microstructure. JAMA Otolaryngology - Head and Neck Surgery, 2020, 146, 1035.	2.2	9
99	The future of digital health with federated learning. Npj Digital Medicine, 2020, 3, 119.	10.9	887
100	Brain connections derived from diffusion MRI tractography can be highly anatomically accurate—if we know where white matter pathways start, where they end, and where they do not go. Brain Structure and Function, 2020, 225, 2387-2402.	2.3	58
101	Thalamocortical Anatomical Connectivity in Schizophrenia and Psychotic Bipolar Disorder. Biological Psychiatry, 2020, 87, S447-S448.	1.3	1
102	Cerebrospinal fluid biomarkers of neurodegeneration, synaptic dysfunction, and axonal injury relate to atrophy in structural brain regions specific to Alzheimer's disease. Alzheimer's and Dementia, 2020, 16, 883-895.	0.8	10
103	A bayesian approach to examining default mode network functional connectivity and cognitive performance in major depressive disorder. Psychiatry Research - Neuroimaging, 2020, 301, 111102.	1.8	1
104	Automatic Labeling of Cortical Sulci Using Spherical Convolutional Neural Networks in a Developmental Cohort. , 2020, 2020, 412-415.		6
105	Mild Cognitive Impairment Staging Yields Genetic Susceptibility, Biomarker, and Neuroimaging Differences. Frontiers in Aging Neuroscience, 2020, 12, 139.	3.4	4
106	A fully automated pipeline for brain structure segmentation in multiple sclerosis. NeuroImage: Clinical, 2020, 27, 102306.	2.7	5
107	Network localization of clinical, cognitive, and neuropsychiatric symptoms in Alzheimer's disease. Brain, 2020, 143, 1249-1260.	7.6	53
108	Multi-path x-D recurrent neural networks for collaborative image classification. Neurocomputing, 2020, 397, 48-59.	5.9	10

4

#	Article	IF	CITATIONS
109	Structural Correlates of the Sensorimotor Cerebellum in Parkinson's Disease and Essential Tremor. Movement Disorders, 2020, 35, 1181-1188.	3.9	18
110	Assessing the Accuracy of a Deep Learning Method to Risk Stratify Indeterminate Pulmonary Nodules. American Journal of Respiratory and Critical Care Medicine, 2020, 202, 241-249.	5.6	109
111	Thalamocortical Anatomical Connectivity in Schizophrenia and Psychotic Bipolar Disorder. Schizophrenia Bulletin, 2020, 46, 1062-1071.	4.3	34
112	CircleNet: Anchor-Free Glomerulus Detection with Circle Representation. Lecture Notes in Computer Science, 2020, 2020, 35-44.	1.3	23
113	Federated Gradient Averaging for Multi-Site Training with Momentum-Based Optimizers. Lecture Notes in Computer Science, 2020, 12444, 170-180.	1.3	10
114	Prediction of Type II Diabetes Onset with Computed Tomography and Electronic Medical Records. Lecture Notes in Computer Science, 2020, 12445, 13-23.	1.3	9
115	Free-water metrics in medial temporal lobe white matter tract projections relate to longitudinal cognitive decline. Neurobiology of Aging, 2020, 94, 15-23.	3.1	23
116	Extracting 2D weak labels from volume labels using multiple instance learning in CT hemorrhage detection. , 2020, 11313, .		4
117	Deep learning estimation of multi-tissue constrained spherical deconvolution with limited single shell DW-MRI. , 2020, 11313, .		11
118	Divergent network properties that predict early surgical failure versus late recurrence in temporal lobe epilepsy. Journal of Neurosurgery, 2020, 132, 1324-1333.	1.6	17
119	Validation and optimization of multi-organ segmentation on clinical imaging archives. , 2020, 11313, .		0
120	Generalizing deep whole-brain segmentation for post-contrast MRI with transfer learning. Journal of Medical Imaging, 2020, 7, 064004.	1.5	4
121	Current Challenges and Future Directions in Diffusion MRI: From Model- to Data- Driven Analysis. Mathematics and Visualization, 2020, , 63-78.	0.6	0
122	Semi-supervised Machine Learning with MixMatch and Equivalence Classes. Lecture Notes in Computer Science, 2020, , 112-121.	1.3	0
123	MRI correlates of chronic symptoms in mild traumatic brain injury. , 2020, 11313, .		1
124	Internal-transfer weighting of multi-task learning for lung cancer detection. , 2020, 11313, .		4
125	Semi-supervised multi-organ segmentation through quality assurance supervision. , 2020, 11313, .		6

126 Contrast phase classification with a generative adversarial network. , 2020, 11313, .

8

#	Article	IF	CITATIONS
127	Outlier guided optimization of abdominal segmentation. , 2020, 11313, .		1
128	Deep multi-task prediction of lung cancer and cancer-free progression from censored heterogenous clinical imaging. , 2020, 11313, .		6
129	Learning from dispersed manual annotations with an optimized data weighting policy. Journal of Medical Imaging, 2020, 7, 1.	1.5	2
130	Correlation of Automated Computed Tomography Volumetric Analysis Metrics With Motility Disturbances in Thyroid Eye Disease. Ophthalmic Plastic and Reconstructive Surgery, 2020, Publish Ahead of Print, 372-376.	0.8	4
131	Generalizing Deep Whole Brain Segmentation for Pediatric and Post- Contrast MRI with Augmented Transfer Learning. Proceedings of SPIE, 2020, 11313, .	0.8	1
132	Semi-supervised Machine Learning with MixMatch and Equivalence Classes. Lecture Notes-monograph Series / Institute of Mathematical Statistics, 2020, 12446, 112-121.	1.0	0
133	Distortion correction of diffusion weighted MRI without reverse phase-encoding scans or field-maps. , 2020, 15, e0236418.		0
134	Distortion correction of diffusion weighted MRI without reverse phase-encoding scans or field-maps. , 2020, 15, e0236418.		0
135	Distortion correction of diffusion weighted MRI without reverse phase-encoding scans or field-maps. , 2020, 15, e0236418.		0
136	Distortion correction of diffusion weighted MRI without reverse phase-encoding scans or field-maps. , 2020, 15, e0236418.		0
137	Distortion correction of diffusion weighted MRI without reverse phase-encoding scans or field-maps. , 2020, 15, e0236418.		0
138	Distortion correction of diffusion weighted MRI without reverse phase-encoding scans or field-maps. , 2020, 15, e0236418.		0
139	A Web-Based Atlas Combining MRI and Histology of the Squirrel Monkey Brain. Neuroinformatics, 2019, 17, 131-145.	2.8	11
140	Disruption of Neural Homeostasis as a Model of Relapse and Recurrence in Late-Life Depression. American Journal of Geriatric Psychiatry, 2019, 27, 1316-1330.	1.2	27
141	Deep learning reveals untapped information for local white-matter fiber reconstruction in diffusion-weighted MRI. Magnetic Resonance Imaging, 2019, 62, 220-227.	1.8	27
142	Diffusion MRI microstructural models in the cervical spinal cord – Application, normative values, and correlations with histological analysis. NeuroImage, 2019, 201, 116026.	4.2	17
143	Fully automatic liver attenuation estimation combing CNN segmentation and morphological operations. Medical Physics, 2019, 46, 3508-3519.	3.0	28
144	Hierarchical spherical deformation for cortical surface registration. Medical Image Analysis, 2019, 57, 72-88.	11.6	27

#	Article	IF	CITATIONS
145	Al in MRI: A case for grassroots deep learning. Magnetic Resonance Imaging, 2019, 64, 1-3.	1.8	5
146	Learning 3D White Matter Microstructure from 2D Histology. , 2019, 2019, 186-190.		0
147	A fiber coherence index for quality control of B-table orientation in diffusion MRI scans. Magnetic Resonance Imaging, 2019, 58, 82-89.	1.8	58
148	Improving human cortical sulcal curve labeling in large scale cross-sectional MRI using deep neural networks. Journal of Neuroscience Methods, 2019, 324, 108311.	2.5	4
149	Anatomical context improves deep learning on the brain age estimation task. Magnetic Resonance Imaging, 2019, 62, 70-77.	1.8	32
150	Assessment of Orbital Computed Tomography (CT) Imaging Biomarkers in Patients with Thyroid Eye Disease. Journal of Digital Imaging, 2019, 32, 987-994.	2.9	10
151	Improved gray matter surface based spatial statistics in neuroimaging studies. Magnetic Resonance Imaging, 2019, 61, 285-295.	1.8	4
152	Multi-modal imaging with specialized sequences improves accuracy of the automated subcortical grey matter segmentation. Magnetic Resonance Imaging, 2019, 61, 131-136.	1.8	3
153	Synthesized b0 for diffusion distortion correction (Synb0-DisCo). Magnetic Resonance Imaging, 2019, 64, 62-70.	1.8	87
154	A deep learning approach to estimation of subject-level bias and variance in high angular resolution diffusion imaging. Magnetic Resonance Imaging, 2019, 59, 130-136.	1.8	1
155	Registration-based image enhancement improves multi-atlas segmentation of the thalamic nuclei and hippocampal subfields. Magnetic Resonance Imaging, 2019, 59, 143-152.	1.8	12
156	Histologically derived fiber response functions for diffusion MRI vary across white matter fibers—An ex vivo validation study in the squirrel monkey brain. NMR in Biomedicine, 2019, 32, e4090.	2.8	16
157	3D whole brain segmentation using spatially localized atlas network tiles. NeuroImage, 2019, 194, 105-119.	4.2	183
158	On-the-fly scheduling versus reservation-based scheduling for unpredictable workflows. International Journal of High Performance Computing Applications, 2019, 33, 1140-1158.	3.7	5
159	Acceleration of spleen segmentation with end-to-end deep learning method and automated pipeline. Computers in Biology and Medicine, 2019, 107, 109-117.	7.0	14
160	Brain structure segmentation in the presence of multiple sclerosis lesions. NeuroImage: Clinical, 2019, 22, 101709.	2.7	15
161	White matter microstructure correlates of general and specific second-order factors of psychopathology. NeuroImage: Clinical, 2019, 22, 101705.	2.7	13
162	Quantitative Spatial Analysis of Metabolic Heterogeneity Across in vivo and in vitro Tumor Models. Frontiers in Oncology, 2019, 9, 1144.	2.8	20

#	Article	IF	CITATIONS
163	Discovering novel disease comorbidities using electronic medical records. PLoS ONE, 2019, 14, e0225495.	2.5	8
164	Functional tractography of white matter by high angular resolution functionalâ€correlation imaging (HARFI). Magnetic Resonance in Medicine, 2019, 81, 2011-2024.	3.0	21
165	Glutamate-sensitive imaging and evaluation of cognitive impairment in multiple sclerosis. Multiple Sclerosis Journal, 2019, 25, 1580-1592.	3.0	22
166	Vascular burden and APOE ε4 are associated with white matter microstructural decline in cognitively normal older adults. NeuroImage, 2019, 188, 572-583.	4.2	48
167	SynSeg-Net: Synthetic Segmentation Without Target Modality Ground Truth. IEEE Transactions on Medical Imaging, 2019, 38, 1016-1025.	8.9	163
168	Splenomegaly Segmentation on Multi-Modal MRI Using Deep Convolutional Networks. IEEE Transactions on Medical Imaging, 2019, 38, 1185-1196.	8.9	35
169	Characterization and correlation of signal drift in diffusion weighted MRI. Magnetic Resonance Imaging, 2019, 57, 133-142.	1.8	6
170	Electronic Medical Record Context Signatures Improve Diagnostic Classification Using Medical Image Computing. IEEE Journal of Biomedical and Health Informatics, 2019, 23, 2052-2062.	6.3	15
171	Harmonization of White and Gray Matter Features in Diffusion Microarchitecture for Cross-Sectional Studies. Lecture Notes in Computational Vision and Biomechanics, 2019, , 21-29.	0.5	2
172	White matter differences between essential tremor and Parkinson disease. Neurology, 2019, 92, e30-e39.	1.1	32
173	Challenges in diffusion MRI tractography – Lessons learned from international benchmark competitions. Magnetic Resonance Imaging, 2019, 57, 194-209.	1.8	99
174	Limits to anatomical accuracy of diffusion tractography using modern approaches. NeuroImage, 2019, 185, 1-11.	4.2	200
175	Intrinsic Functional Network Connectivity Is Associated With Clinical Symptoms and Cognition in Late-Life Depression. Biological Psychiatry: Cognitive Neuroscience and Neuroimaging, 2019, 4, 160-170.	1.5	30
176	Anatomical accuracy of standard-practice tractography algorithms in the motor system - A histological validation in the squirrel monkey brain. Magnetic Resonance Imaging, 2019, 55, 7-25.	1.8	36
177	Structural covariance across the lifespan: Brain development and aging through the lens of interâ€network relationships. Human Brain Mapping, 2019, 40, 125-136.	3.6	24
178	Inter-Scanner Harmonization of High Angular Resolution DW-MRI Using Null Space Deep Learning. Mathematics and Visualization, 2019, , 193-201.	0.6	14
179	Enabling Multi-shell b-Value Generalizability of Data-Driven Diffusion Models with Deep SHORE. Lecture Notes in Computer Science, 2019, 11766, 573-581.	1.3	5
180	Distanced LSTM: Time-Distanced Gates in Long Short-Term Memory Models for Lung Cancer Detection. Lecture Notes in Computer Science, 2019, , 310-318.	1.3	28

#	Article	IF	CITATIONS
181	Stochastic tissue window normalization of deep learning on computed tomography. Journal of Medical Imaging, 2019, 6, 1.	1.5	11
182	Using deep learning for a diffusion-based segmentation of the dentate nucleus and its benefits over atlas-based methods. Journal of Medical Imaging, 2019, 6, 1.	1.5	4
183	Towards machine learning prediction of deep brain stimulation (DBS) intra-operative efficacy maps. , 2019, 10949, .		11
184	Distributed deep learning for robust multi-site segmentation of CT imaging after traumatic brain injury. , 2019, 10949, .		12
185	Coronary calcium detection using 3D attention identical dual deep network based on weakly supervised learning. , 2019, 10949, .		9
186	Improving splenomegaly segmentation by learning from heterogeneous multi-source labels. , 2019, 10949, .		14
187	Lung cancer detection using co-learning from chest CT images and clinical demographics. , 2019, 10949, .		16
188	Contextual Deep Regression Network for Volume Estimation in Orbital CT. Lecture Notes in Computer Science, 2019, 11769, 104-111.	1.3	1
189	Cortical Surface Parcellation Using Spherical Convolutional Neural Networks. Lecture Notes in Computer Science, 2019, 11766, 501-509.	1.3	17
190	Reproducibility evaluation of SLANT whole brain segmentation across clinical magnetic resonance imaging protocols. , 2019, 10949, .		6
191	Quantitative assessment of dMRI-based dentate-rubro-thalamic tractography in squirrel monkey. , 2019, , .		0
192	Montage based 3D medical image retrieval from traumatic brain injury cohort using deep convolutional neural network. , 2019, 10949, .		2
193	Consideration of cerebrospinal fluid intensity variation in diffusion weighted MRI. , 2019, 10948, .		0
194	Harmonizing 1.5T/3T diffusion weighted MRI through development of deep learning stabilized microarchitecture estimators. , 2019, 10949, .		5
195	Abstract 3317: Development of a lung nodule cohort with integrated clinical, molecular and imaging biomarkers. , 2019, , .		0
196	Distanced LSTM: Time-Distanced Gates in Long Short-Term Memory Models for Lung Cancer Detection. , 2019, 11861, 310-318.		7
197	Inter-Scanner Harmonization of High Angular Resolution DW-MRI using Null Space Deep Learning. Lecture Notes-monograph Series / Institute of Mathematical Statistics, 2019, 2019, 193-201.	1.0	2
198	Robust Multicontrast MRI Spleen Segmentation for Splenomegaly Using Multi-Atlas Segmentation. IEEE Transactions on Biomedical Engineering, 2018, 65, 336-343.	4.2	22

#	Article	IF	CITATIONS
199	TRACE: A Topological Graph Representation for Automatic Sulcal Curve Extraction. IEEE Transactions on Medical Imaging, 2018, 37, 1653-1663.	8.9	20
200	Empirical single sample quantification of bias and variance in Qâ€ball imaging. Magnetic Resonance in Medicine, 2018, 80, 1666-1675.	3.0	3
201	Confirmation of a gyral bias in diffusion <scp>MRI</scp> fiber tractography. Human Brain Mapping, 2018, 39, 1449-1466.	3.6	105
202	Towards Portable Large-Scale Image Processing with High-Performance Computing. Journal of Digital Imaging, 2018, 31, 304-314.	2.9	23
203	Empirical reproducibility, sensitivity, and optimization of acquisition protocol, for Neurite Orientation Dispersion and Density Imaging using AMICO. Magnetic Resonance Imaging, 2018, 50, 96-109.	1.8	16
204	Tests of cortical parcellation based on white matter connectivity using diffusion tensor imaging. NeuroImage, 2018, 170, 321-331.	4.2	13
205	Histological validation of diffusion MRI fiber orientation distributions and dispersion. NeuroImage, 2018, 165, 200-221.	4.2	156
206	Prefrontal-Thalamic Anatomical Connectivity and Executive Cognitive Function in Schizophrenia. Biological Psychiatry, 2018, 83, 509-517.	1.3	145
207	Splenomegaly segmentation using global convolutional kernels and conditional generative adversarial networks. , 2018, 10574, .		29
208	Technology Enablers for Big Data, Multi-Stage Analysis in Medical Image Processing. , 2018, , .		1
209	Why rankings of biomedical image analysis competitions should be interpreted with care. Nature Communications, 2018, 9, 5217.	12.8	198
210	A data colocation grid framework for big data medical image processing: backend design. , 2018, 10597, .		4
211	Learning implicit brain MRI manifolds with deep learning. , 2018, 10574, .		51
212	Less is More: Simultaneous View Classification and Landmark Detection for Abdominal Ultrasound Images. Lecture Notes in Computer Science, 2018, , 711-719.	1.3	24
213	F82. Latent Factors of Psychopathology and Functional Connectivity of the Dorsal Anterior Cingulate Cortex During Reward Anticipation. Biological Psychiatry, 2018, 83, S269-S270.	1.3	0
214	T222. Functional Brain Activation and Grey Matter Integrity in Psychosis: A Combined Functional Magnetic Resonance and Neurite Orientation Distribution and Density Imaging Study. Biological Psychiatry, 2018, 83, S214-S215.	1.3	1
215	Hierarchical Spherical Deformation for Shape Correspondence. Lecture Notes in Computer Science, 2018, 11070, 853-861.	1.3	0
216	How to Exploit Weaknesses in Biomedical Challenge Design and Organization. Lecture Notes in Computer Science, 2018, , 388-395.	1.3	10

#	Article	IF	CITATIONS
217	Multi-atlas Parcellation in the Presence of Lesions: Application to Multiple Sclerosis. Lecture Notes in Computer Science, 2018, , 104-113.	1.3	2
218	Relating structural and functional brainstem connectivity to disease measures in epilepsy. Neurology, 2018, 91, e67-e77.	1.1	48
219	Assessing the inter-observer variability of Computer-Aided Nodule Assessment and Risk Yield (CANARY) to characterize lung adenocarcinomas. PLoS ONE, 2018, 13, e0198118.	2.5	9
220	Right Fronto-Subcortical White Matter Microstructure Predicts Cognitive Control Ability on the Go/No-go Task in a Community Sample. Frontiers in Human Neuroscience, 2018, 12, 127.	2.0	8
221	Comparing fully automated state-of-the-art cerebellum parcellation from magnetic resonance images. NeuroImage, 2018, 183, 150-172.	4.2	80
222	Fully convolutional neural networks improve abdominal organ segmentation. , 2018, 10574, .		34
223	Adversarial synthesis learning enables segmentation without target modality ground truth. , 2018, , .		78
224	Spatially Localized Atlas Network Tiles Enables 3D Whole Brain Segmentation from Limited Data. Lecture Notes in Computer Science, 2018, , 698-705.	1.3	16
225	Automated Characterization of Body Composition and Frailty with Clinically Acquired CT. Lecture Notes in Computer Science, 2018, 10734, 25-35.	1.3	12
226	Empirical estimation of intravoxel structure with persistent angular structure and Q-ball models of diffusion weighted MRI. Journal of Medical Imaging, 2018, 5, 1.	1.5	6
227	Sulcal depth-based cortical shape analysis in normal healthy control and schizophrenia groups. , 2018, 10574, .		12
228	SHARD: spherical harmonic-based robust outlier detection for HARDI methods. , 2018, 10574, .		2
229	Phantom-based field maps for gradient nonlinearity correction in diffusion imaging. , 2018, 10573, .		8
230	Tests of clustering thalamic nuclei based on various dMRI models in the squirrel monkey brain. , 2018, 10578, .		0
231	Constructing statistically unbiased cortical surface templates using feature-space covariance. , 2018, 10574, .		0
232	Improved stability of whole brain surface parcellation with multi-atlas segmentation. , 2018, 10574, .		4
233	Evaluation of inter-site bias and variance in diffusion-weighted MRI. , 2018, 10574, .		1
234	Quadratic: quality of dice in registration circuits. , 2018, 10574, .		2

#	Article	IF	CITATIONS
235	Abstract 2191: Quantitative cell-level spatial analysis of tumor metabolism. , 2018, , .		0
236	Imaging biomarkers in thyroid eye disease and their clinical associations. Journal of Medical Imaging, 2018, 5, 1.	1.5	1
237	Improved automatic optic nerve radius estimation from high resolution MRI. Proceedings of SPIE, 2017, 10133, .	0.8	2
238	Multi-scale hippocampal parcellation improves atlas-based segmentation accuracy. Proceedings of SPIE, 2017, 10133, .	0.8	10
239	Effects of b-value and number of gradient directions on diffusion MRI measures obtained with Q-ball imaging. Proceedings of SPIE, 2017, 10133, .	0.8	16
240	Structural-functional relationships between eye orbital imaging biomarkers and clinical visual assessments. , 2017, 10133, .		4
241	Comparison of multi-fiber reproducibility of PAS-MRI and Q-ball with empirical multiple b-value HARDI. Proceedings of SPIE, 2017, 10133, .	0.8	6
242	Multi-atlas segmentation enables robust multi-contrast MRI spleen segmentation for splenomegaly. , 2017, 10133, .		5
243	Multi-atlas spleen segmentation on CT using adaptive context learning. Proceedings of SPIE, 2017, 10133,	0.8	9
244	Cloud Engineering Principles and Technology Enablers for Medical Image Processing-as-a-Service. , 2017, 2017, 127-137.		7
245	Algorithmic Enhancements to Big Data Computing Frameworks for Medical Image Processing. , 2017, , .		5
246	Empirical consideration of the effects of acquisition parameters and analysis model on clinically feasible q-ball imaging. Magnetic Resonance Imaging, 2017, 40, 62-74.	1.8	7
247	Magnetic resonance imaging connectivity for the prediction of seizure outcome in temporal lobe epilepsy. Epilepsia, 2017, 58, 1251-1260.	5.1	62
248	Convergent individual differences in visual cortices, but not the amygdala across standard amygdalar fMRI probe tasks. NeuroImage, 2017, 146, 312-319.	4.2	7
249	Stability of gradient field corrections for quantitative diffusion MRI. Proceedings of SPIE, 2017, 10132, .	0.8	11
250	Deep learning for brain tumor classification. Proceedings of SPIE, 2017, , .	0.8	95
251	Theoretical and empirical comparison of big data image processing with Apache Hadoop and Sun Grid Engine. Proceedings of SPIE, 2017, 10138, .	0.8	5
252	Spinal cord grey matter segmentation challenge. NeuroImage, 2017, 152, 312-329.	4.2	97

#	Article	IF	CITATIONS
253	DAX - the next generation: towards one million processes on commodity hardware. , 2017, 2017, .		3
254	Phenotype analysis of early risk factors from electronic medical records improves image-derived diagnostic classifiers for optic nerve pathology. , 2017, 10138, .		2
255	Automated Characterization of Pyelocalyceal Anatomy Using CT Urograms to Aid in Management of Kidney Stones. Lecture Notes in Computer Science, 2017, , 99-107.	1.3	1
256	Can increased spatial resolution solve the crossing fiber problem for diffusion MRI?. NMR in Biomedicine, 2017, 30, e3787.	2.8	61
257	Quantitative characterization of optic nerve atrophy in patients with multiple sclerosis. Multiple Sclerosis Journal - Experimental, Translational and Clinical, 2017, 3, 205521731773009.	1.0	8
258	957. Neurite Orientation Dispersion and Density Imaging (NODDI) of the Prefrontal Cortex in Psychosis. Biological Psychiatry, 2017, 81, S387.	1.3	0
259	820. Latent Factors of Psychopathology and Grey Matter Volume. Biological Psychiatry, 2017, 81, S333.	1.3	0
260	The VALiDATe29 MRI Based Multi-Channel Atlas of the Squirrel Monkey Brain. Neuroinformatics, 2017, 15, 321-331.	2.8	23
261	Density-based clustering analyses to identify heterogeneous cellular sub-populations. , 2017, , .		1
262	Simultaneous total intracranial volume and posterior fossa volume estimation using multiâ€atlas label fusion. Human Brain Mapping, 2017, 38, 599-616.	3.6	32
263	Reproducibility and variation of diffusion measures in the squirrel monkey brain, in vivo and ex vivo. Magnetic Resonance Imaging, 2017, 35, 29-38.	1.8	22
264	[ICâ€Pâ€143]: SOFTWARE COMPARISONS FOR SUBCORTICAL MEASUREMENTS IN HEALTHY OLDER ADULTS ACROSS ADNI AND PPMI. Alzheimer's and Dementia, 2017, 13, P108.	0.8	0
265	Comparison of Cortical and Subcortical Measurements in Normal Older Adults across Databases and Software Packages. Journal of Alzheimer's Disease Reports, 2017, 1, 59-70.	2.2	7
266	Gray Matter Surface Based Spatial Statistics (GS-BSS) in Diffusion Microstructure. Lecture Notes in Computer Science, 2017, 10433, 638-646.	1.3	13
267	Multiprotocol, multiatlas statistical fusion: theory and application. Journal of Medical Imaging, 2017, 4, 1.	1.5	2
268	EMR-Radiological Phenotypes in Diseases of the Optic Nerve and Their Association with Visual Function. Lecture Notes in Computer Science, 2017, 2017, 373-381.	1.3	4
269	4D Multi-atlas Label Fusion Using Longitudinal Images. Lecture Notes in Computer Science, 2017, 10530, 3-11.	1.3	3
270	Multi-modal and targeted imaging improves automated mid-brain segmentation. , 2017, 10133, .		3

#	Article	IF	CITATIONS
271	Abstract 3723: Assessing the reproducibility of computer-aided nodule assessment and risk yield (CANARY) method to characterize lung adenocarcinomas. , 2017, , .		1
272	Quantifying the impact of underlying measurement error on cervical spinal cord diffusion tensor imaging at 3T. Journal of Magnetic Resonance Imaging, 2016, 44, 1608-1618.	3.4	11
273	Structural functional associations of the orbit in thyroid eye disease: Kalman filters to track extraocular rectal muscles. Proceedings of SPIE, 2016, 9784, .	0.8	8
274	Cortical Implications of Advancing Age and Disease Duration in Parkinson's Disease Patients with Postural Instability and Gait Dysfunction. Journal of Parkinson's Disease, 2016, 6, 441-451.	2.8	18
275	Combining multi-atlas segmentation with brain surface estimation. Proceedings of SPIE, 2016, 9784, .	0.8	18
276	A Bayesian framework for early risk prediction in traumatic brain injury. Proceedings of SPIE, 2016, 9784, .	0.8	6
277	Improving cerebellar segmentation with statistical fusion. Proceedings of SPIE, 2016, 9784, .	0.8	5
278	Whole abdominal wall segmentation using augmented active shape models (AASM) with multi-atlas label fusion and level set. , 2016, 9784, .		2
279	On the fallacy of quantitative segmentation for T1-weighted MRI. , 2016, 9784, .		4
280	Abdomen and spinal cord segmentation with augmented active shape models. Journal of Medical Imaging, 2016, 3, 036002.	1.5	5
281	Cortical asymmetry in Parkinson's disease: early susceptibility of the left hemisphere. Brain and Behavior, 2016, 6, e00573.	2.2	79
282	Improving Spleen Volume Estimation Via Computer-assisted Segmentation on Clinically Acquired CT Scans. Academic Radiology, 2016, 23, 1214-1220.	2.5	9
283	A 3D high resolution ex vivo white matter atlas of the common squirrel monkey (saimiri sciureus) based on diffusion tensor imaging. , 2016, 9784, .		10
284	Evaluation of body-wise and organ-wise registrations for abdominal organs. Proceedings of SPIE, 2016, 9784, .	0.8	4
285	Performance management of high performance computing for medical image processing in Amazon Web Services. , 2016, 9789, .		6
286	Evaluation of Six Registration Methods for the Human Abdomen on Clinically Acquired CT. IEEE Transactions on Biomedical Engineering, 2016, 63, 1563-1572.	4.2	111
287	Short term reproducibility of a high contrast 3-D isotropic optic nerve imaging sequence in healthy controls. , 2016, 9783, .		4
288	The Attenuation Distribution Across the Long Axis (ADLA). Academic Radiology, 2016, 23, 718-723.	2.5	3

#	Article	IF	CITATIONS
289	Consistent cortical reconstruction and multi-atlas brain segmentation. NeuroImage, 2016, 138, 197-210.	4.2	94
290	Peripheral sphingolipids are associated with variation in white matter microstructure in older adults. Neurobiology of Aging, 2016, 43, 156-163.	3.1	16
291	Vanderbilt University Institute of Imaging Science Center for Computational Imaging XNAT: A multimodal data archive and processing environment. NeuroImage, 2016, 124, 1097-1101.	4.2	38
292	Disambiguating the optic nerve from the surrounding cerebrospinal fluid: Application to MSâ€related atrophy. Magnetic Resonance in Medicine, 2016, 75, 414-422.	3.0	11
293	Comparison of 3D orientation distribution functions measured with confocal microscopy and diffusion MRI. NeuroImage, 2016, 129, 185-197.	4.2	85
294	Lower gray matter integrity is associated with greater lap time variation in high-functioning older adults. Experimental Gerontology, 2016, 77, 46-51.	2.8	4
295	The effect of age and microstructural white matter integrity on lap time variation and fast-paced walking speed. Brain Imaging and Behavior, 2016, 10, 697-706.	2.1	21
296	Mapping Lifetime Brain Volumetry with Covariate-Adjusted Restricted Cubic Spline Regression from Cross-Sectional Multi-site MRI. Lecture Notes in Computer Science, 2016, 9900, 81-88.	1.3	14
297	Linear and Curvilinear Trajectories of Cortical Loss with Advancing Age and Disease Duration in Parkinson's Disease. , 2016, 7, 220.		12
298	Investigation of Bias in Continuous Medical Image Label Fusion. PLoS ONE, 2016, 11, e0155862.	2.5	2
299	Integration of the Java Image Science Toolkit with E-Science Platform. The Insight Journal, 2016, , .	0.2	Ο
300	Quantitative CT Imaging of Ventral Hernias: Preliminary Validation of an Anatomical Labeling Protocol. PLoS ONE, 2015, 10, e0141671.	2.5	13
301	Efficient multi-atlas abdominal segmentation on clinically acquired CT with SIMPLE context learning. Medical Image Analysis, 2015, 24, 18-27.	11.6	84
302	Efficient abdominal segmentation on clinically acquired CT with SIMPLE context learning. Proceedings of SPIE, 2015, 9413, .	0.8	3
303	Evaluation of five image registration tools for abdominal CT: pitfalls and opportunities with soft anatomy. , 2015, 9413, .		8
304	Constructing a statistical atlas of the radii of the optic nerve and cerebrospinal fluid sheath in young healthy adults. , 2015, 9413, .		7
305	Bootstrapping white matter segmentation, Eve++. , 2015, 9413, .		6
306	Revealing latent value of clinically acquired CTs of traumatic brain injury through multi-atlas segmentation in a retrospective study of 1,003 with external cross-validation. Proceedings of SPIE, 2015, 9413, .	0.8	5

#	Article	IF	CITATIONS
307	Integrating histology and MRI in the first digital brain of common squirrel monkey, Saimiri sciureus. , 2015, 9417, .		4
308	Toward content-based image retrieval with deep convolutional neural networks. Proceedings of SPIE, 2015, 9417, .	0.8	25
309	Voxelwise Relationships Between Distribution Volume Ratio and Cerebral Blood Flow: Implications for Analysis of β-Amyloid Images. Journal of Nuclear Medicine, 2015, 56, 1042-1047.	5.0	11
310	Multi-atlas segmentation for abdominal organs with Gaussian mixture models. , 2015, 9417, .		4
311	Heritability of fractional anisotropy in human white matter: A comparison of Human Connectome Project and ENIGMA-DTI data. NeuroImage, 2015, 111, 300-311.	4.2	227
312	Multi-atlas learner fusion: An efficient segmentation approach for large-scale data. Medical Image Analysis, 2015, 26, 82-91.	11.6	32
313	Region of interest correction factors improve reliability of diffusion imaging measures within and across scanners and field strengths. NeuroImage, 2015, 119, 406-416.	4.2	48
314	Robust optic nerve segmentation on clinically acquired CT. , 2014, 9034, 90341G.		6
315	A brain MRI atlas of the common squirrel monkey,Saimiri sciureus. , 2014, 9038, 90380C.		12
316	Impact of family structure and common environment on heritability estimation for neuroimaging genetics studies using Sequential Oligogenic Linkage Analysis Routines. Journal of Medical Imaging, 2014, 1, 014005.	1.5	12
317	On study design in neuroimaging heritability analyses. , 2014, , .		0
318	Applying the algorithm "assessing quality using image registration circuits" (AQUIRC) to multi-atlas segmentation. , 2014, , .		1
319	Shape-constrained multi-atlas segmentation of spleen in CT. Proceedings of SPIE, 2014, 9034, 903446.	0.8	12
320	Robust optic nerve segmentation on clinically acquired computed tomography. Journal of Medical Imaging, 2014, 1, 034006.	1.5	30
321	Selfâ€assessed performance improves statistical fusion of image labels. Medical Physics, 2014, 41, 031903.	3.0	3
322	Combining meta- and mega- analytic approaches for multi-site diffusion imaging based genetic studies: From the ENIGMA-DTI working group. , 2014, , .		0
323	Statistical label fusion with hierarchical performance models. , 2014, 9034, 90341E.		18
324	Evaluation of multiatlas label fusion forin vivomagnetic resonance imaging orbital segmentation. Journal of Medical Imaging, 2014, 1, 024002.	1.5	14

#	Article	IF	CITATIONS
325	SIMPLE Is a Good Idea (and Better with Context Learning). Lecture Notes in Computer Science, 2014, 17, 364-371.	1.3	10
326	Evaluation of Statistical Inference on Empirical Resting State fMRI. IEEE Transactions on Biomedical Engineering, 2014, 61, 1091-1099.	4.2	8
327	The ENIGMA Consortium: large-scale collaborative analyses of neuroimaging and genetic data. Brain Imaging and Behavior, 2014, 8, 153-182.	2.1	696
328	Hierarchical performance estimation in the statistical label fusion framework. Medical Image Analysis, 2014, 18, 1070-1081.	11.6	36
329	Multisurgeon, Multisite Validation of a Trajectory Planning Algorithm for Deep Brain Stimulation Procedures. IEEE Transactions on Biomedical Engineering, 2014, 61, 2479-2487.	4.2	25
330	Groupwise multi-atlas segmentation of the spinal cord's internal structure. Medical Image Analysis, 2014, 18, 460-471.	11.6	49
331	Validating DICOM Transcoding with an Open Multi-Format Resource. Neuroinformatics, 2014, 12, 615-617.	2.8	1
332	Resource Estimation in High Performance Medical Image Computing. Neuroinformatics, 2014, 12, 563-573.	2.8	5
333	Multi-site study of additive genetic effects on fractional anisotropy of cerebral white matter: Comparing meta and megaanalytical approaches for data pooling. NeuroImage, 2014, 95, 136-150.	4.2	127
334	Assessment of bias in experimentally measured diffusion tensor imaging parameters using SIMEX. Magnetic Resonance in Medicine, 2013, 69, 891-902.	3.0	15
335	Non-local statistical label fusion for multi-atlas segmentation. Medical Image Analysis, 2013, 17, 194-208.	11.6	191
336	Correcting power and p-value calculations for bias in diffusion tensor imaging. Magnetic Resonance Imaging, 2013, 31, 857-864.	1.8	4
337	Multi-site genetic analysis of diffusion images and voxelwise heritability analysis: A pilot project of the ENICMA–DTI working group. NeuroImage, 2013, 81, 455-469.	4.2	354
338	System for Integrated Neuroimaging Analysis and Processing of Structure. Neuroinformatics, 2013, 11, 91-103.	2.8	20
339	Functional Networks in Temporal-Lobe Epilepsy: A Voxel-Wise Study of Resting-State Functional Connectivity and Gray-Matter Concentration. Brain Connectivity, 2013, 3, 22-30.	1.7	32
340	Approaching expert results using a hierarchical cerebellum parcellation protocol for multiple inexpert human raters. Neurolmage, 2013, 64, 616-629.	4.2	32
341	Robust non-local multi-atlas segmentation of the optic nerve. Proceedings of SPIE, 2013, 8669, 86691L.	0.8	9
342	Quantitative anatomical labeling of the anterior abdominal wall. Proceedings of SPIE, 2013, 8673, 867312.	0.8	6

#	Article	IF	CITATIONS
343	Immersive virtual reality for visualization of abdominal CT. Proceedings of SPIE, 2013, 8673, .	0.8	19
344	Automatic segmentation of abdominal wall in ventral hernia CT: a pilot study. , 2013, 8669, .		3
345	Robust inter-modality multi-atlas segmentation for PACS-based DTI quality control. , 2013, 8674, .		2
346	Integration of XNAT/PACS, DICOM, and research software for automated multi-modal image analysis. , 2013, 8674, .		15
347	Texture analysis improves level set segmentation of the anterior abdominal wall. Medical Physics, 2013, 40, 121901.	3.0	10
348	Outâ€ofâ€atlas likelihood estimation using multiâ€atlas segmentation. Medical Physics, 2013, 40, 043702.	3.0	12
349	Simultaneous Analysis and Quality Assurance for Diffusion Tensor Imaging. PLoS ONE, 2013, 8, e61737.	2.5	60
350	Robust GM/WM Segmentation of the Spinal Cord with Iterative Non-local Statistical Fusion. Lecture Notes in Computer Science, 2013, 16, 759-767.	1.3	10
351	Whole Brain Functional Connectivity Using Multi-scale Spatio-Spectral Random Effects Model. Lecture Notes in Computer Science, 2013, , 170-179.	1.3	0
352	Collaborative labeling of malignant glioma. , 2012, 2012, 1148-1151.		2
353	Out-of-atlas labeling: A multi-atlas approach to cancer segmentation. , 2012, 2012, 1236-1239.		6
354	Automating PACS quality control with the Vanderbilt image processing enterprise resource. , 2012, 8319, .		2
355	Generalized statistical label fusion using multiple consensus levels. , 2012, 8314, .		0
356	A comparison of distributional considerations with statistical analysis of resting state fMRI at 3T and 7T. , 2012, 8314, .		10
357	Collaborative labeling of malignant glioma with WebMILL: a first look. Proceedings of SPIE, 2012, 8318, ·	0.8	0
358	Baseline Cardiovascular Risk Predicts Subsequent Changes in Resting Brain Function. Stroke, 2012, 43, 1542-1547.	2.0	39
359	Finding seeds for segmentation using statistical fusion. , 2012, 8314, .		2

360 Simultaneous segmentation and statistical label fusion. , 2012, 8314, .

#	Article	IF	CITATIONS
361	Towards automatic quantitative quality control for MRI. , 2012, 8314, .		5
362	Segmentation of malignant gliomas through remote collaboration and statistical fusion. Medical Physics, 2012, 39, 5981-5989.	3.0	2
363	Magnetic Resonance Connectome Automated Pipeline: An Overview. IEEE Pulse, 2012, 3, 42-48.	0.3	24
364	Formulating Spatially Varying Performance in the Statistical Fusion Framework. IEEE Transactions on Medical Imaging, 2012, 31, 1326-1336.	8.9	95
365	Correction to "Formulating Spatially Varying Performance in the Statistical Fusion Framework" [Jun 12 1326-1336]. IEEE Transactions on Medical Imaging, 2012, 31, 1505-1505.	8.9	Ο
366	Foibles, follies, and fusion: Web-based collaboration for medical image labeling. NeuroImage, 2012, 59, 530-539.	4.2	11
367	Resolution of crossing fibers with constrained compressed sensing using diffusion tensor MRI. NeuroImage, 2012, 59, 2175-2186.	4.2	115
368	Biological parametric mapping accounting for random regressors with regression calibration and model II regression. Neurolmage, 2012, 62, 1761-1768.	4.2	5
369	A surgeon specific automatic path planning algorithm for deep brain stimulation. , 2012, , .		11
370	MRI Shows a Region-Specific Pattern of Atrophy in Spinocerebellar Ataxia Type 2. Cerebellum, 2012, 11, 272-279.	2.5	49
371	Robust Statistical Fusion of Image Labels. IEEE Transactions on Medical Imaging, 2012, 31, 512-522.	8.9	38
372	Non-local STAPLE: An Intensity-Driven Multi-atlas Rater Model. Lecture Notes in Computer Science, 2012, 15, 426-434.	1.3	30
373	Do We Really Need Robust and Alternative Inference Methods for Brain MRI?. Lecture Notes in Computer Science, 2012, , 77-93.	1.3	1
374	Quantitative Evaluation of Statistical Inference in Resting State Functional MRI. Lecture Notes in Computer Science, 2012, 15, 246-253.	1.3	2
375	Next Ceneration of the Java Image Science Toolkit (JIST): Visualization and Validation. The Insight Journal, 2012, 2012, 1-16.	0.2	7
376	Next Generation of the JAVA Image Science Toolkit (JIST) Visualization and Validation. The Insight Journal, 2012, , .	0.2	1
377	Biological parametric mapping with robust and non-parametric statistics. NeuroImage, 2011, 57, 423-430.	4.2	40
378	Multi-parametric neuroimaging reproducibility: A 3-T resource study. Neurolmage, 2011, 54, 2854-2866.	4.2	318

#	Article	IF	CITATIONS
379	Assessment of Bias for MRI Diffusion Tensor Imaging Using SIMEX. Lecture Notes in Computer Science, 2011, 14, 107-115.	1.3	6
380	Robust Statistical Label Fusion Through Consensus Level, Labeler Accuracy, and Truth Estimation (COLLATE). IEEE Transactions on Medical Imaging, 2011, 30, 1779-1794.	8.9	73
381	Development of chemical exchange saturation transfer at 7T. Magnetic Resonance in Medicine, 2011, 66, 831-838.	3.0	88
382	A framework on surface-based connectivity quantification for the human brain. Journal of Neuroscience Methods, 2011, 197, 324-332.	2.5	6
383	Statistical fusion of continuous labels: identification of cardiac landmarks. Proceedings of SPIE, 2011, 7962, .	0.8	8
384	Foibles, follies, and fusion: assessment of statistical label fusion techniques for web-based collaborations using minimal training. , 2011, 7962, 79623G.		4
385	Robust biological parametric mapping: an improved technique for multimodal brain image analysis. Proceedings of SPIE, 2011, 7962, 79623X.	0.8	6
386	Integrating medical imaging analyses through a high-throughput bundled resource imaging system. Proceedings of SPIE, 2011, 7967, .	0.8	1
387	Effect of regularization parameter and scan time on crossing fibers with constrained compressed sensing. Proceedings of SPIE, 2011, 7962, 79624J.	0.8	3
388	Characterizing and optimizing rater performance for internet-based collaborative labeling. , 2011, 7966, .		4
389	Characterizing Spatially Varying Performance to Improve Multi-atlas Multi-label Segmentation. Lecture Notes in Computer Science, 2011, 22, 85-96.	1.3	34
390	Accounting for Random Regressors: A Unified Approach to Multi-modality Imaging. Lecture Notes in Computer Science, 2011, 7012, 1-9.	1.3	1
391	Complex geometric models of diffusion and relaxation in healthy and damaged white matter. NMR in Biomedicine, 2010, 23, 152-162.	2.8	29
392	Reproducibility of tractâ€specific magnetization transfer and diffusion tensor imaging in the cervical spinal cord at 3 tesla. NMR in Biomedicine, 2010, 23, 207-217.	2.8	59
393	Diffusion tensor imaging reveals disease-specific deep cerebellar nuclear changes in cerebellar degeneration. Journal of Neurology, 2010, 257, 1406-1408.	3.6	8
394	The Java Image Science Toolkit (JIST) for Rapid Prototyping and Publishing of Neuroimaging Software. Neuroinformatics, 2010, 8, 5-17.	2.8	121
395	<i>q</i> â€space and conventional diffusion imaging of axon and myelin damage in the rat spinal cord after axotomy. Magnetic Resonance in Medicine, 2010, 63, 1323-1335.	3.0	43
396	5.5: Presentation session: Neuroscience informatics: "Interfaces and integration of Medical Image Analysis frameworks: Challenges and opportunities". , 2010, , .		0

#	Article	IF	CITATIONS
397	Simultaneous truth and performance level estimation with incomplete, over-complete, and ancillary data. Proceedings of SPIE, 2010, 7623, 76231N.	0.8	10
398	Statistical fusion of surface labels provided by multiple raters. , 2010, 7623, .		8
399	Resolution of crossing fibers with constrained compressed sensing using traditional diffusion tensor MRI. , 2010, 7623, 76231H.		20
400	Interfaces and integration of medical image analysis frameworks: Challenges and opportunities. , 2010, 2010, 1-4.		2
401	Water saturation shift referencing (WASSR) for chemical exchange saturation transfer (CEST) experiments. Magnetic Resonance in Medicine, 2009, 61, 1441-1450.	3.0	555
402	Robust estimation of spatially variable noise fields. Magnetic Resonance in Medicine, 2009, 62, 500-509.	3.0	30
403	Orthogonal diffusion-weighted MRI measures distinguish region-specific degeneration in cerebellar ataxia subtypes. Journal of Neurology, 2009, 256, 1939-1942.	3.6	16
404	Estimation and application of spatially variable noise fields in diffusion tensor imaging. Magnetic Resonance Imaging, 2009, 27, 741-751.	1.8	32
405	Effect of oral appliances on genioglossus muscle tonicity seen with diffusion tensor imaging: A pilot study. Oral Surgery Oral Medicine Oral Pathology Oral Radiology and Endodontics, 2009, 107, e57-e63.	1.4	14
406	Diffusion tensor imaging at low SNR: nonmonotonic behaviors of tensor contrasts. Magnetic Resonance Imaging, 2008, 26, 790-800.	1.8	40
407	Automatically identifying white matter tracts using cortical labels. , 2008, , 895.		3
408	Regional Differences in Diffusion Tensor Imaging Measurements: Assessment of Intrarater and Interrater Variability. American Journal of Neuroradiology, 2008, 29, 1124-1127.	2.4	39
409	Tongue muscle fiber tracking during rest and tongue protrusion with oral appliances: A preliminary study with diffusion tensor imaging. Acoustical Science and Technology, 2008, 29, 291-294.	0.5	18
410	Effects of diffusion weighting schemes on the reproducibility of DTI-derived fractional anisotropy, mean diffusivity, and principal eigenvector measurements at 1.5T. NeuroImage, 2007, 36, 1123-1138.	4.2	266
411	Diffusion Tensor Estimation by Maximizing Rician Likelihood. , 2007, , 1-8.		27
412	Effects of signalâ€ŧoâ€noise ratio on the accuracy and reproducibility of diffusion tensor imaging–derived fractional anisotropy, mean diffusivity, and principal eigenvector measurements at 1.5T. Journal of Magnetic Resonance Imaging, 2007, 26, 756-767.	3.4	336
413	Statistical parametric mapping of brain morphology: Sensitivity is dramatically increased by using brain-extracted images as inputs. NeuroImage, 2006, 30, 1187-1195.	4.2	56
414	Brain atrophy in long-term abstinent alcoholics who demonstrate impairment on a simulated gambling task. NeuroImage, 2006, 32, 1465-1471.	4.2	92

#	Article	IF	CITATIONS
415	Treated and treatment-naive alcoholics come from different populations. Alcohol, 2005, 35, 19-26.	1.7	64
416	The Pathophysiology of ???Brain Shrinkage??? in Alcoholics ??? Structural and Molecular Changes and Clinical Implications. Alcoholism: Clinical and Experimental Research, 2005, 29, 1106-1115.	2.4	15
417	Treated and treatment-naive alcoholics come from different populations. Alcohol, 2005, 36, 19-26.	1.7	20
418	Controlling for premorbid brain size in imaging studies: T1-derived cranium scaling factor vs. T2-derived intracranial vault volume. Psychiatry Research - Neuroimaging, 2004, 131, 169-176.	1.8	22
419	COGNITIVE FUNCTION AND ???BRAIN SHRINKAGE??? IN LONG-TERM ABSTINENT ALCOHOLICS Alcoholism: Clinical and Experimental Research, 2004, 28, 79A.	2.4	0